Joint Active and Passive Beamforming for NLOS Target Detection in RIS-Assisted Mono-Static Radar

Cengcang Zeng, Yifan Liang, and Hongbin Li
Department of Electrical and Computer Engineering
Stevens Institute of Technology
Hoboken, NJ 07030, USA

***Abstract*—Reconfigurable intelligent surfaces (RIS) have gained widespread application in the field of communications and are gradually extending their utility to the radar domain. This paper focuses on a mono-static RIS-assisted radar system. The problem is to jointly design the active beamformer for the radar and passive beamformer for the RIS. We begin by introducing a general signal model. In order to enhance target illumination and echo reception, we maximize the received signal power through the optimization of both the radar beamformer and the phase-shift matrix for the RIS. We provide a closed-form solution for the resulting optimization problem. The proposed RIS-assisted radar is employed for non-line-of sight (NLOS) target detection, where the radar is obstructed from the target. A statistical analysis of the detection performance is presented. Simulation results underscore the significant impact of RIS size and radar-RIS distance on detection performance. Moreover, we demonstrate that RIS can offer a practical solution for NLOS target detection.**

***Index Terms*—Non-line-of-sight (NLOS) target, reconfigurable intelligent surface (RIS), joint active and passive beamforming, target detection**

I. Introduction

Reconfigurable intelligent surfaces (RIS) represent an emerging and promising technology that has garnered increasing attention in recent years, particularly in the context of next-generation communication systems (such as those beyond 5G and in anticipation of future 6G) and sensing applications [1]–[5]. RIS is a cost-effective, nearly passive planar structure capable of precise control over the electric field properties of incoming signals, including phase, amplitude, frequency, and polarization [6]. This capability allows RIS to steer incident electromagnetic waves toward arbitrary directions or specific locations, similar to the functionality of phased arrays [7]. This enhancement significantly improves signal reception at desired destinations.

Although a significant portion of prior studies on RIS focused on the field of communication, recent investigations in the radar domain have delved into the application of RIS to address a variety of radar signal-related challenges. Specifically, one of the directions of studies focuses on the integration of RIS into Dual-function Radar and Communication (DFRC) systems [8]–[11]. In [8], the dual-functional transmit waveform and the passive beamforming design of RIS was used to maximize the radar output signal-to-interference-plus-noise ratio. In [9] and [10] the RIS was utilized to improve target detection in environments with severe path loss and obtain better beampattern matches with the target transmit beampattern, respectively. While [11] employed the RIS to mitigate mutual interference. Another direction focuses on utilizing RIS to enhance the detection performance in radar systems [12]–[14]. In particular, [12] examined the use of RIS with multi-input multi-output (MIMO) radar in various configurations. Meanwhile, [13] further considered the effect of asynchronous propagation in RIS-assisted MIMO radar, where the radar signals propagate through different paths (i.e., direct path and RIS paths) and arrive at the receiver at different times. Clutter mitigation using RIS was studied in [14].

Conventional radar relies heavily on line-of-sight (LOS) paths between the transmitter and target and between the target and receiver. However, surveillance environments, particularly in urban and indoor settings, present considerable challenges due to various obstructive elements like walls and moving objects such as pedestrians and vehicles [15]. To tackle these challenges, one approach is to employ radar networks. For instance, [16] proposed a distributed radar system to establish continuous coverage in urbanized regions. Alternatively, a more cost-effective solution involves leveraging IRS technology. Specifically, [17] conducted an analysis of the impact of RIS on radar equations for surveillance in non-line of sight (NLOS) scenarios. Joint active and passive beamforming was employed in [18] to improve the detection of the NLOS targets. Additionally, in [19], the deployment of multiple RIS platforms created a virtual or NLOS link to enhance radar performance.

In this paper, we commence by introducing a mono-static RIS-assisted system and establish the corresponding signal model. Our objective is to maximize received signal power to facilitate target illumination and echo reception. Consequently, we formulate the associated optimization problem and provide a closed-form solution. Furthermore, we consider target detection using the proposed RIS-assisted radar and conduct a statistical analysis of the detector, yielding closed-form expressions for both the probability of false alarm and the probability of detection. In our simulations, we first investigate the impact of RIS size and the distance between RIS and the radar on detection performance within a NLOS environment. Subsequently, we reaffirm the influence of RIS size and TX-RIS distance by comparing the variation in detection performance at different target positions within the same NLOS

This work was supported in part by the National Science Foundation under grants CCF-2316865, ECCS-1923739, ECCS-2212940, and ECCS-2332534.

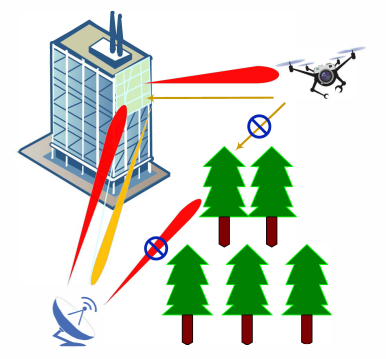

Figure 1. A mono-static radar with an RIS employed to assist NLOS target illumination and observation.

environment. Through the target detection performance map, we demonstrate that RIS can offer a viable solution to assist target detection in NLOS scenarios.

II. Signal Model and Problem Formulation

We consider a mono-static RIS-assisted radar system for NLOS target detection, as depicted in Fig. 1, where an RIS is employed to assist target illumination and echo receiving. The radar is equipped with N antennas and the RIS comprises M meta-atoms. We use $\psi_m \in [0, 2\pi]$ to represent the phase shift associated with the m-th element of the RIS. The diagonal matrix accounting for the phase response of the RIS can be expressed as

$$\boldsymbol{\Psi} \triangleq \text{diag}(e^{j\psi_1}, \cdots, e^{j\psi_M}). \tag{1}$$

After matched filtering and sampling, the received signal at the receiver can be represented as:

$$z = \alpha\sqrt{P_\text{t}}\boldsymbol{w}^T\boldsymbol{H}_{\text{r,s}}^T\boldsymbol{\Psi}\boldsymbol{h}_{\text{s,a}}\boldsymbol{h}_{\text{s,a}}^T\boldsymbol{\Psi}\boldsymbol{H}_{\text{r,s}}\boldsymbol{w} + \epsilon, \tag{2}$$

where the scalar $\sqrt{P_\text{t}}$ is to ensure the total radar transmit power is P_t and

- α: complex target amplitude
- $\boldsymbol{h}_{\text{s,a}} \in \mathbb{C}^{M\times 1}$: RIS-target channel
- $\boldsymbol{H}_{\text{r,s}} \in \mathbb{C}^{M\times N}$: radar-RIS channel
- $\boldsymbol{w} \in \mathbb{C}^{N\times 1}$: TX beamforming vector with unit-norm $\|\boldsymbol{w}\| = 1$
- ϵ: Gaussian noise with zero mean and variance σ_n^2

The system comprises cascade connections of several one-hop sub-channels represented in Fig. 2. These sub-channels include $\boldsymbol{H}_{\text{r,s}}$ and $\boldsymbol{h}_{\text{s,a}}$ for the forward transmission process as well as their transposes for the backward receiving process. The forward channels can be modeled as:

$$\boldsymbol{H}_{\text{r,s}} = \rho_{\text{r,s}}\boldsymbol{a}_\text{s}(\boldsymbol{\phi}_{\text{r,s}})\boldsymbol{a}_\text{r}^H(\boldsymbol{\theta}_{\text{r,s}}), \tag{3}$$

$$\boldsymbol{h}_{\text{s,a}}^T = \rho_{\text{s,a}}\boldsymbol{a}_\text{s}^H(\boldsymbol{\theta}_{\text{s,a}}), \tag{4}$$

$$\rho_{\text{r,s}} = \left(\frac{G_\text{r}(\boldsymbol{\theta}_{\text{r,s}})A_\text{s}}{4\pi R_{\text{r,s}}^2 L_{\text{r,s}}}\right)^{1/2} e^{-\jmath 2\pi R_{\text{r,s}}/\lambda}, \tag{5}$$

$$\rho_{\text{s,a}} = \left(\frac{G_\text{s}(\boldsymbol{\theta}_{\text{s,a}})}{4\pi R_{\text{s,a}}^2 L_{\text{s,a}}}\right)^{1/2} e^{-\jmath 2\pi R_{\text{s,a}}/\lambda}, \tag{6}$$

where

- G_r: antenna gain of the radar
- G_s: antenna gain of an RIS element as a reflector
- $A_\text{s} = \lambda^2/4$: effective area of an RIS element where the elements are $\lambda/2$ away from each other[1]
- $L_{\text{r,s}}$ and $L_{\text{s,a}}$: total path loss (e.g., transmit loss, atmospheric loss, receiver loss, signal processing loss, RIS loss, etc.) associated with the radar-RIS and RIS-target links, respectively
- $R_{\text{r,s}}$ and $R_{\text{s,a}}$: propagation distance across different channels
- $\boldsymbol{a}_\text{r}(\boldsymbol{\theta})$: TX steering vector with angles of departure (AoDs) $\boldsymbol{\theta}$ that may combine both the angle in azimuth and angle in elevation
- $\boldsymbol{a}_\text{s}(\boldsymbol{\phi})$, $\boldsymbol{a}_\text{s}(\boldsymbol{\theta})$: RIS steering vector with angles of arrival (AoAs) $\boldsymbol{\phi}$ and AoDs $\boldsymbol{\theta}$, respectively

Suppose the RIS employs an $M = N_x \times N_y$ uniform planar array (UPA) with uniform inter-element separation of d_x and d_y in the x- and y-direction. The RIS steering vector can be expressed as

$$\boldsymbol{a}_\text{s}(\boldsymbol{\vartheta}) = \boldsymbol{a}_{\text{s},y}(u_y) \otimes \boldsymbol{a}_{\text{s},x}(u_x), \tag{7}$$

where $\boldsymbol{\vartheta} = [\vartheta_x, \vartheta_y]$ with ϑ_x denoting the azimuth AoD or AoA, while ϑ_y denoting the elevation AoD or AoA. The steering vectors in the x- and y-direction are given by

$$\boldsymbol{a}_{\text{s},x}(u_x) = [1, e^{\jmath 2\pi u_x}, \cdots, e^{\jmath 2\pi u_x(N_x-1)}], \tag{8}$$

$$\boldsymbol{a}_{\text{s},y}(u_y) = [1, e^{\jmath 2\pi u_y}, \cdots, e^{\jmath 2\pi u_y(N_y-1)}], \tag{9}$$

which are directly parameterized by the 2D spatial frequencies:

$$u_y = \frac{d_y}{\lambda}\sin(\vartheta_y)\cos(\vartheta_x), \tag{10}$$

$$u_x = \frac{d_x}{\lambda}\sin(\vartheta_y)\sin(\vartheta_x). \tag{11}$$

Meanwhile, if the radar employs an $N \times 1$ uniform linear array (ULA) with uniform antenna separation of d. The radar steering vector can be expressed as

$$\boldsymbol{a}_\text{r}(\theta) = [1, e^{\jmath 2\pi u}, \cdots, e^{\jmath 2\pi u(N-1)}], \tag{12}$$

where $u = \frac{d}{\lambda}\sin(\theta)$.

III. Joint Radar and RIS Beamforming Design

For the joint design problem, we consider selecting the radar beamformer $\boldsymbol{w}$ and RIS phase matrix $\boldsymbol{\Psi}$ to make the power of the received signal as large as possible. For this purpose, we can let the radar beamformer $\boldsymbol{w}$ to maximize the total target illumination power for any RIS phase matrix $\boldsymbol{\Psi}$. This is because the received target power is maximized only when the target illumination power is maximized. The target illumination power is proportional to $\|\boldsymbol{h}_{\text{s,a}}^T\boldsymbol{\Psi}\boldsymbol{H}_{\text{r,s}}\boldsymbol{w}\|^2$. Hence, we have

$$\hat{\boldsymbol{w}} = \arg \max_{\boldsymbol{w}} \left\|\boldsymbol{h}_{\text{s,a}}^T\boldsymbol{\Psi}\boldsymbol{H}_{\text{r,s}}\boldsymbol{w}\right\|^2 \quad \text{s.t.} \quad \|\boldsymbol{w}\|^2 = 1. \tag{13}$$

[1]Note that the effective area is in general dependent on the incident angle. For simplicity, it is herein modeled as a constant.

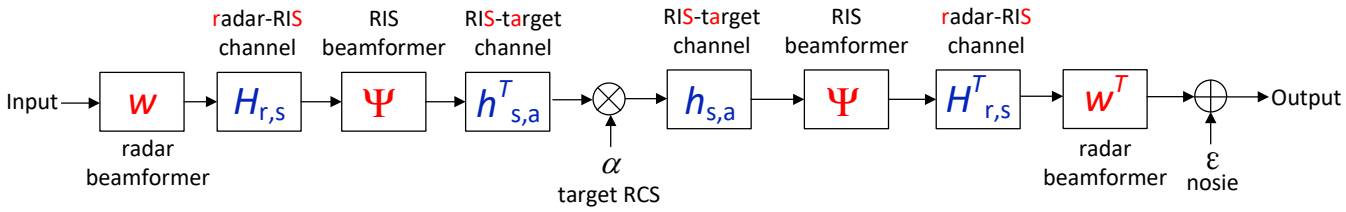

Figure 2. Mathematical representation of a mono-static radar assisted with RIS.

Clearly, the optimum radar beamformer is the principal eigenvector of the rank-1 matrix $\boldsymbol{H}_{\mathrm{r,s}}^H\boldsymbol{\Psi}^H\boldsymbol{h}_{\mathrm{s,a}}^*\boldsymbol{h}_{\mathrm{s,a}}^T\boldsymbol{\Psi}\boldsymbol{H}_{\mathrm{r,s}}$, which is also a matched filter given by

$$\hat{\boldsymbol{w}} = \frac{\boldsymbol{H}_{\mathrm{r,s}}^H\boldsymbol{\Psi}^H\boldsymbol{h}_{\mathrm{s,a}}^*}{\|\boldsymbol{H}_{\mathrm{r,s}}^H\boldsymbol{\Psi}^H\boldsymbol{h}_{\mathrm{s,a}}^*\|}. \tag{14}$$

Using the above radar beamformer, the received signal can be expressed as

$$z = \alpha\sqrt{P_{\mathrm{t}}}\|\boldsymbol{H}_{\mathrm{r,s}}^H\boldsymbol{\Psi}^H\boldsymbol{h}_{\mathrm{s,a}}^*\|^2 + \epsilon. \tag{15}$$

The received signal power is given by

$$y = |\alpha|^2 P_{\mathrm{t}}\|\boldsymbol{H}_{\mathrm{r,s}}^H\boldsymbol{\Psi}^H\boldsymbol{h}_{\mathrm{s,a}}^*\|^4. \tag{16}$$

The RIS beamformer can be designed by maximizing the received signal power

$$\begin{aligned} \max_{\boldsymbol{\Psi}} \quad & \|\boldsymbol{H}_{\mathrm{r,s}}^H\boldsymbol{\Psi}^H\boldsymbol{h}_{\mathrm{s,a}}^*\|^4 \\ \text{s.t.} \quad & \boldsymbol{\Psi} = \mathrm{diag}(e^{j\psi_1}, \cdots, e^{j\psi_M}). \end{aligned} \tag{17}$$

Recalling that the radar-RIS channel $\boldsymbol{H}_{\mathrm{r,s}}$ is identified as a rank-one matrix in (3), by incorporating this into the objective function specified in (17), we can obtain

$$\begin{aligned} &\|\boldsymbol{H}_{\mathrm{r,s}}^H\boldsymbol{\Psi}^H\boldsymbol{h}_{\mathrm{s,a}}^*\|^4 \\ =&|\boldsymbol{h}_{\mathrm{s,a}}^T\boldsymbol{\Psi}\boldsymbol{H}_{\mathrm{r,s}}\boldsymbol{H}_{\mathrm{r,s}}^H\boldsymbol{\Psi}^H\boldsymbol{h}_{\mathrm{s,a}}^*|^2 \\ =&|\rho_{\mathrm{r,s}}|^4|\rho_{\mathrm{s,a}}|^4|\boldsymbol{\psi}^T\boldsymbol{s}\boldsymbol{a}_{\mathrm{r}}^H(\boldsymbol{\theta}_{\mathrm{r,s}})\boldsymbol{a}_{\mathrm{r}}(\boldsymbol{\theta}_{\mathrm{r,s}})\boldsymbol{s}^H\boldsymbol{\psi}^*|^2 \\ =&N^2|\rho_{\mathrm{r,s}}|^4|\rho_{\mathrm{s,a}}|^4|\boldsymbol{\psi}^T\boldsymbol{s}\boldsymbol{s}^H\boldsymbol{\psi}^*|^2, \end{aligned} \tag{18}$$

where

$$\boldsymbol{s} = \mathrm{diag}\big(\boldsymbol{a}_{\mathrm{s}}^*(\boldsymbol{\theta}_{\mathrm{s,a}})\big)\boldsymbol{a}_{\mathrm{s}}(\boldsymbol{\phi}_{\mathrm{r,s}}), \tag{19}$$

and

$$\boldsymbol{\psi} \triangleq [e^{j\psi_1}, \cdots, e^{j\psi_M}]^T. \tag{20}$$

Referring to (18), the optimization problem (17) can be simplified as

$$\hat{\boldsymbol{\psi}} = \arg\max_{\boldsymbol{\psi}} \boldsymbol{\psi}^T\boldsymbol{s}\boldsymbol{s}^H\boldsymbol{\psi}^*, \tag{21}$$

and the solution is given by

$$\hat{\boldsymbol{\psi}} = [e^{-j\arg(s_1)}, \cdots, e^{-j\arg(s_M)}]^T, \tag{22}$$

where $\arg(x)$ represents the argument of the complex number x and s_m denotes the m-th entry of $\boldsymbol{s}$.

IV. Target Detection

Now we consider NLOS target detection using the RIS-aided radar. We first simplify (2) by using the optimal radar beamformer $\hat{\boldsymbol{w}}$ and RIS phase vector $\hat{\boldsymbol{\psi}}$ in the equation. Then, the received signal can be rewritten as

$$\begin{aligned} z &= \alpha\sqrt{P_{\mathrm{t}}}\hat{\boldsymbol{w}}^T\boldsymbol{H}_{\mathrm{r,s}}^T\hat{\boldsymbol{\Psi}}\boldsymbol{h}_{\mathrm{s,a}}\boldsymbol{h}_{\mathrm{s,a}}^T\hat{\boldsymbol{\Psi}}\boldsymbol{H}_{\mathrm{r,s}}\hat{\boldsymbol{w}} + \epsilon \\ &= \alpha\sqrt{P_{\mathrm{t}}}\|\boldsymbol{H}_{\mathrm{r,s}}^H\hat{\boldsymbol{\Psi}}^H\boldsymbol{h}_{\mathrm{s,a}}^*\|^2 + \epsilon \\ &= \alpha N\sqrt{P_{\mathrm{t}}}|\rho_{\mathrm{r,s}}|^2|\rho_{\mathrm{s,a}}|^2\hat{\boldsymbol{\psi}}^T\boldsymbol{s}\boldsymbol{s}^H\hat{\boldsymbol{\psi}}^* + \epsilon \\ &= \alpha NM^2\sqrt{P_{\mathrm{t}}}|\rho_{\mathrm{r,s}}|^2|\rho_{\mathrm{s,a}}|^2 + \epsilon, \end{aligned} \tag{23}$$

The target detection problem is described by the following hypothesis testing:

$$\begin{aligned} &\mathcal{H}_0 : z = \epsilon, \\ &\mathcal{H}_1 : z = \alpha NM^2\sqrt{P_{\mathrm{t}}}|\rho_{\mathrm{r,s}}|^2|\rho_{\mathrm{s,a}}|^2 + \epsilon, \end{aligned} \tag{24}$$

where $\mathcal{H}_0$ and $\mathcal{H}_1$ represent the target-absent and, respectively, target-present state.

A simple detector for the hypothesis testing is given by

$$T = |z| \underset{\mathcal{H}_0}{\overset{\mathcal{H}_1}{\gtrless}} \gamma. \tag{25}$$

Under $\mathcal{H}_0$, z is a complex Gaussian random variable with zero mean and variance σ_n^2, i.e., $z \sim \mathcal{CN}(0, \sigma_n^2)$. Therefore, T is a Rayleigh distribution under $\mathcal{H}_0$ with probability density function (PDF) given by

$$p_T(t|\mathcal{H}_0) = \frac{2t}{\sigma_n^2}e^{-\frac{t^2}{\sigma_n^2}}, \ t \geq 0. \tag{26}$$

Under $\mathcal{H}_1$, z is a complex Gaussian random variable with non-zero mean $\alpha NM^2\sqrt{P_{\mathrm{t}}}|\rho_{\mathrm{r,s}}|^2|\rho_{\mathrm{s,a}}|^2$ and variance σ_n^2, i.e., $\Re\{z\} \sim \mathcal{N}(\Re\{\alpha\}NM^2\sqrt{P_{\mathrm{t}}}|\rho_{\mathrm{r,s}}|^2|\rho_{\mathrm{s,a}}|^2, \sigma_n^2/2)$ and $\Im\{z\} \sim \mathcal{N}(\Im\{\alpha\}NM^2\sqrt{P_{\mathrm{t}}}|\rho_{\mathrm{r,s}}|^2|\rho_{\mathrm{s,a}}|^2, \sigma_n^2/2)$, Hence, T is a Rician distribution under $\mathcal{H}_1$, given by

$$p_T(t|\mathcal{H}_1) = \frac{2t}{\sigma_n^2}e^{-\frac{1}{\sigma_n^2}(t^2+\beta^2)}I_0\Big(\frac{2\beta t}{\sigma_n^2}\Big), \ t \geq 0, \tag{27}$$

where $\beta^2 = |\alpha|^2N^2M^4P_{\mathrm{t}}|\rho_{\mathrm{r,s}}|^4|\rho_{\mathrm{s,a}}|^4$. Based on the above analysis, the probability of false alarm (P_f) can be calculated as

$$P_f = \int_{\gamma}^{\infty} p_T(t|\mathcal{H}_0)dt = e^{\frac{-\gamma^2}{\sigma_n^2}}. \tag{28}$$

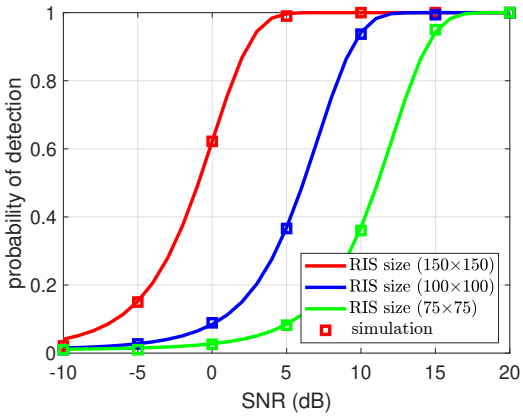

Figure 3. Probability of detection versus SNR with different RIS array size

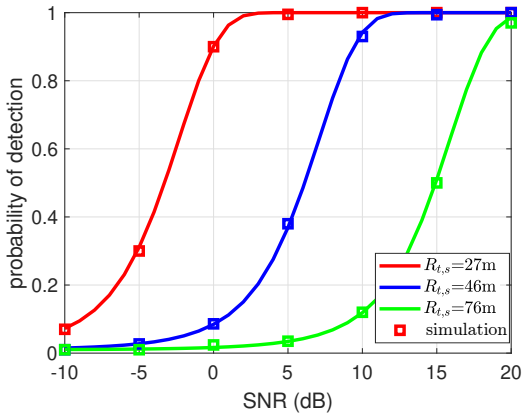

Figure 4. Probability of detection versus SNR for different TX-RIS distances

Then, the threshold can be obtained in terms of P_f

$$\gamma = \sqrt{-\sigma_n^2 \ln P_f}. \tag{29}$$

Similarly, the probability of detection (P_d) is obtained

$$\begin{aligned} P_d &= \int_{\gamma}^{\infty} p_T(t|\mathcal{H}_1)dt \\ &= \int_{\gamma}^{\infty} \frac{2t}{\sigma_n^2} e^{-\frac{1}{\sigma_n^2}(t^2+\beta^2)} I_0\Big(\frac{2\beta t}{\sigma_n^2}\Big) \\ &= Q\left(\sqrt{\frac{2|\alpha|^2 N^2 M^4 P_{\mathrm{t}} |\rho_{\mathrm{r,s}}|^4 |\rho_{\mathrm{s,a}}|^4}{\sigma_n^2}}, \sqrt{\frac{2\gamma^2}{\sigma_n^2}}\right). \end{aligned} \tag{30}$$

V. Numerical Results

In this section, we employ simulation results to demonstrate the influence of RIS on detection performance. The simulation scenario involves a mono-static RIS-assisted radar system with one radar and one RIS. The radar is a ULA equipped with 64 antennas ($N = 64$). The RIS is a UPA consisting of $M = N_x \times N_y$ meta-atoms. Additionally, the target has a radar cross-section (RCS) of $0.02\mathrm{m}^2$. The transmit power $P_{\mathrm{t}} = 20\mathrm{W}$, the carrier frequency is 3 GHz, the noise variance $\sigma_n^2 = -90\mathrm{dBm}$, and the probability of false alarm is $P_f = 10^{-2}$. The SNR is defined as

$$\mathrm{SNR} = \frac{|\alpha|^2 N^2 M^4 P_{\mathrm{t}} |\rho_{\mathrm{r,s}}|^4 |\rho_{\mathrm{s,a}}|^4}{\sigma_n^2}. \tag{31}$$

First, we examine the impact of the size of the RIS, denoted as M. We assume that the positions of the radar, RIS, and target are fixed to isolate the effects of other factors. We considered three sizes for the RIS: $M = 75 \times 75$, $M = 100 \times 100$, and $M = 150 \times 150$. The inter-element spacing is $d_x = d_y = \lambda/2 = 0.015\mathrm{m}$, and the RIS occupies areas of approximately $0.5625\mathrm{m}^2$, $1\mathrm{m}^2$, and $2.25\mathrm{m}^2$, respectively. Fig. 3 illustrates the probability of detection P_d versus SNR for the radar with three different RIS sizes. P_d is determined using both the theoretical analysis in Section IV and simulations, and the results from both methods are observed to be in agreement. When comparing the detection performance of the three RIS specifications, it becomes evident that as the RIS size increases, the detection performance improves significantly.

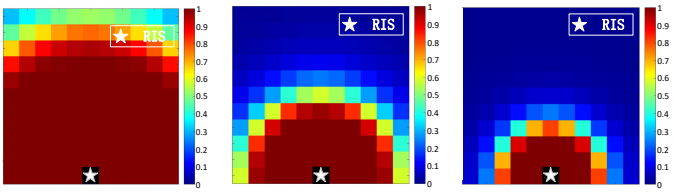

(a) (b) (c)

Figure 5. Target detection performance map with the x-axis ranging from -50m to 50m and the y-axis ranging from 0m to 100m (a) RIS size 200×200 (b) RIS size 100×100 (c) RIS size 75×75

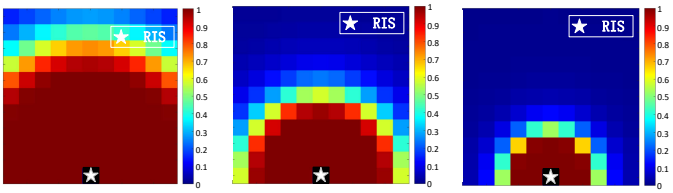

(a) (b) (c)

Figure 6. Target detection performance map with the x-axis ranging from -50m to 50m and the y-axis ranging from 0m to 100m (a) TX-RIS distance 27m (b) TX-RIS distance 46m (c) TX-RIS distance 76m

Next, the impact of the TX-RIS distance, denoted as $R_{\mathrm{t,s}}$, is examined. In this case, we keep the size of the RIS fixed at $M = 100 \times 100$. To simplify the setup, we maintain the radar's coordinates at $[0, 0, 0]\mathrm{m}$ and also fix the positions of the RIS. This allows us to vary the SNR by altering the positions of the target. We analyze the detection performance in three different geometric setups: when the RIS is located at $[0, 25, 10]\mathrm{m}$, $[0, 45, 10]\mathrm{m}$, and $[0, 75, 10]\mathrm{m}$. Fig. 4 presents the probability of detection P_d versus SNR for the radar with different TX-RIS distances, respectively. Similarly, P_d is determined through theoretical analysis and simulations in Section IV, and the results from both methods remain consistent. As depicted in Fig. 4, it is evident that there is a substantial improvement in detection performance when the RIS is closer to the TX. Conversely, an increase in the TX-RIS distance leads to a

noticeable decrease in detection performance. This observation highlights the significant impact of the TX-RIS distance on the detection performance.

To further investigate the impact of RIS on detection performance in the NLOS scenario, we consider a scenario where the target moves arbitrarily within a 100m$\times$100m area, and this area is entirely obstructed from the radar's perspective. The positions of the radar and the RIS remain fixed, with the radar located at $[0, -45, 0]$m and the RIS positioned at $[0, 0, 6]$m, resulting in a fixed TX-RIS distance of 45.3m. Simultaneously, we set the target to vary its position on a plane at a height of 3m. Fig. 5 presents a target detection performance map, with the x-axis ranging from -50m to 50m and the y-axis ranging from 0m to 100m. By comparing the target detection performance at different locations, we can clearly determine whether we can detect the presence of targets at these various positions. Furthermore, by comparing the detection performance maps in Fig. 5(a), (b), and (c) for different RIS sizes, we can once again confirm that larger RIS sizes significantly enhance our ability to detect the presence of targets. In general, radar target detection relies heavily on the existence of LOS paths between the transmitter and the target. Based on the aforementioned observations, we can conclude that RIS can provide a viable solution for scenarios where LOS paths are obstructed, such as NLOS situations.

Lastly, in the same NLOS scenario within a 100m$\times$100m area, we examined the target detection performance map while varying the TX-RIS distance under a constant RIS size $M = 100 \times 100$. Specifically, we investigated the detection performance at three different distances: 27m, 46m, and 76m. By comparing the results in Fig. 6, we can reaffirm that as the distance decreases, our ability to detect targets improves, and the variation in distance significantly impacts target detection performance.

VI. Conclusion

In this paper, we have discussed a mono-static radar system assisted by RIS and introduced the corresponding signal model. Leveraging this model, we have proposed a closed-form solution to joint radar and RIS beamforming design to maximize the received signal power, thereby assisting detection performance. Also, the detection performance is presented through a statistical analysis. Our investigation begins by examining factors affecting target detection performance, including RIS size and radar-RIS distance. Additionally, we have explored a NLOS scenario and our analysis includes detection performance maps illustrating target detection capabilities at various locations. Simulation results confirm that both RIS size and radar-RIS distance have a significant impact on detection performance. Moreover, our findings indicate that in NLOS scenarios, the use of RIS to assist with target illumination and echo reception offers a practical and effective solution for NLOS target detection.

References

[1] M. A. ElMossallamy, H. Zhang, L. Song, K. G. Seddik, Z. Han, and G. Y. Li, "Reconfigurable intelligent surfaces for wireless communications: Principles, challenges, and opportunities," *IEEE Transactions on Cognitive Communications and Networking*, vol. 6, no. 3, pp. 990–1002, 2020.

[2] Y. Liu, X. Liu, X. Mu, T. Hou, J. Xu, M. Di Renzo, and N. Al-Dhahir, "Reconfigurable intelligent surfaces: Principles and opportunities," *IEEE communications surveys & tutorials*, vol. 23, no. 3, pp. 1546–1577, 2021.

[3] W. Lu, B. Deng, Q. Fang, X. Wen, and S. Peng, "Intelligent reflecting surface-enhanced target detection in MIMO radar," *IEEE Sensors Letters*, vol. 5, no. 2, pp. 1–4, 2021.

[4] C. Pan, H. Ren, K. Wang, J. F. Kolb, M. Elkashlan, M. Chen, M. Di Renzo, Y. Hao, J. Wang, A. L. Swindlehurst *et al.*, "Reconfigurable intelligent surfaces for 6G systems: Principles, applications, and research directions," *IEEE Communications Magazine*, vol. 59, no. 6, pp. 14–20, 2021.

[5] P. Wang, J. Fang, H. Duan, and H. Li, "Compressed channel estimation for intelligent reflecting surface-assisted millimeter wave systems," *IEEE signal processing letters*, vol. 27, pp. 905–909, 2020.

[6] S. Basharat, S. A. Hassan, H. Pervaiz, A. Mahmood, Z. Ding, and M. Gidlund, "Reconfigurable intelligent surfaces: Potentials, applications, and challenges for 6G wireless networks," *IEEE Wireless Communications*, vol. 28, no. 6, pp. 184–191, 2021.

[7] S. Buzzi, E. Grossi, M. Lops, and L. Venturino, "Radar target detection aided by reconfigurable intelligent surfaces," *IEEE Signal Processing Letters*, vol. 28, pp. 1315–1319, 2021.

[8] R. Liu, M. Li, Y. Liu, Q. Wu, and Q. Liu, "Joint transmit waveform and passive beamforming design for RIS-aided DFRC systems," *IEEE Journal of Selected Topics in Signal Processing*, vol. 16, no. 5, pp. 995–1010, 2022.

[9] Z.-M. Jiang, M. Rihan, P. Zhang, L. Huang, Q. Deng, J. Zhang, and E. M. Mohamed, "Intelligent reflecting surface aided dual-function radar and communication system," *IEEE Systems Journal*, vol. 16, no. 1, pp. 475–486, 2021.

[10] X. Wang, Z. Fei, Z. Zheng, and J. Guo, "Joint waveform design and passive beamforming for RIS-assisted dual-functional radar-communication system," *IEEE Transactions on Vehicular Technology*, vol. 70, no. 5, pp. 5131–5136, 2021.

[11] Y. He, Y. Cai, H. Mao, and G. Yu, "RIS-assisted communication radar coexistence: Joint beamforming design and analysis," *IEEE Journal on Selected Areas in Communications*, vol. 40, no. 7, pp. 2131–2145, 2022.

[12] S. Buzzi, E. Grossi, M. Lops, and L. Venturino, "Foundations of MIMO radar detection aided by reconfigurable intelligent surfaces," *IEEE Transactions on Signal Processing*, vol. 70, pp. 1749–1763, 2022.

[13] F. Wang, A. L. Swindlehurst, and H. Li, "Detection performance of RIS-Aided MIMO radar with asynchronous propagation," in *2023 IEEE International Workshop on Computational Advances in Multi-Sensor Adaptive Processing (CAMSAP 2023), DECEMBER 10-13, 2023, LOS SUEOS, COSTA RICA*, 2023.

[14] F. Wang, H. Li, and A. L. Swindlehurst, "Clutter suppression for target detection using hybrid reconfigurable intelligent surfaces," in *2023 IEEE Radar Conference (RadarConf23), May 1-5, 2023, San Antonio, Texas*, 2023, pp. 1–5.

[15] O. Rabaste, J. Bosse, D. Poullin, I. D. H. Sáenz, T. Letertre, T. Chonavel *et al.*, "Detection-localization algorithms in the around-the-corner radar problem," *IEEE Transactions on Aerospace and Electronic Systems*, vol. 55, no. 6, pp. 2658–2673, 2019.

[16] X. Guo, C. S. Ng, E. de Jong, and A. B. Smits, "Concept of distributed radar system for mini-UAV detection in dense urban environment," in *2019 International Radar Conference (RADAR)*. IEEE, 2019, pp. 1–4.

[17] A. Aubry, A. De Maio, and M. Rosamilia, "Reconfigurable intelligent surfaces for N-LOS radar surveillance," *IEEE Transactions on Vehicular Technology*, vol. 70, no. 10, pp. 10 735–10 749, 2021.

[18] F. Wang, H. Li, and J. Fang, "Joint active and passive beamforming for IRS-Assisted radar," *IEEE Signal Processing Letters*, vol. 29, pp. 349–353, 2022.

[19] Z. Esmaeilbeig, K. V. Mishra, and M. Soltanalian, "IRS-Aided radar: Enhanced target parameter estimation via intelligent reflecting surfaces," in *2022 IEEE 12th Sensor Array and Multichannel Signal Processing Workshop (SAM)*, 2022, pp. 286–290.